Available online at www.sciencedirect.com
SCIENCE DIRECT®
Optics Communications 213 (2002) 103–119
OPTICS COMMUNICATIONS
www.elsevier.com/locate/optcom

Environmentally induced noises in an actively mode-locked erbium fibre laser operating in the second-order rational harmonic mode locking regime

O. Pottiez*, P. Mégret, M. Blondel

Service d'Electromagnétisme et de Télécommunications, Faculté Polytechnique de Mons, Boulevard Dolez 31, B-7000 Mons, Belgium

Received 7 August 2002; received in revised form 9 September 2002; accepted 15 September 2002

Abstract

We investigate the influence of environmentally induced cavity length fluctuations on the energy and phase noises of an optical pulse train generated by an actively mode-locked erbium-doped fibre laser that is operated in the second-order rational harmonic mode-locking regime. Using a simple model that was recently proposed to describe this particular regime, we identify the specific nature of these energy and phase noises, and we demonstrate that their values averaged over two consecutive pulses in the train can be measured directly by implementing the time-domain demodulation technique. For a known cavity length variation, we compare the values of the average energy and phase fluctuations that are obtained both theoretically, using the model, and experimentally, through time-domain demodulation. This study brings out a mechanism of coupling between the energy and phase fluctuations that appears when cavity length fluctuations are at play. This coupling is caused by the periodic intracavity amplitude modulation and strongly depends on the average detuning of the cavity length. Through the measurement of the cross-correlation between energy and phase noises, we identify environmental perturbations as a major source of the noises that affect a pulse train generated through second-order rational harmonic mode locking.

PACS: 42.60.Mi; 42.55.Wd; 42.60.Fc

Keywords: Laser noise; Mode-locked fibre laser; Active mode-locking; Optical pulse generation

1. Introduction

It is now widely accepted that actively mode-locked erbium-doped fibre lasers are valuable sources of high-speed picosecond pulse trains that deserve a foreground status in applications such as fast optical telecommunications and all-optical analog-to-digital conversion. In order to reach the multigigahertz repetition rates that are required by these applications, this type of laser must be driven at a modulation frequency f_m corresponding to a large integer multiple N of the cavity resonance

* Corresponding author. Tel.: +32-65-37-41-44; fax: +32-65-37-41-99.
E-mail address: pottiez@telecom.fpms.ac.be (O. Pottiez).

0030-4018/02/$ - see front matter
PII: S0030-4018(02)02074-6

frequency, or free spectral range (FSR), which lies typically in the megahertz range only. When this very common technique, called harmonic mode locking, is used, the repetition rate f_p of the generated pulse train is always equal to f_m, so that the ultimate limitation to the repetition rate is imposed by the electrical bandwidth of the driving electronics, including the radio-frequency (RF) generator, the electrooptic modulator, and other RF elements. This situation becomes particularly harmful when repetition rates of several tens of gigahertz or more are targeted. In order to overcome this limitation, the technique of rational harmonic mode locking (RHML) was introduced [1]. Indeed, when this technique is employed, the repetition rate of the generated pulse train is an integer multiple P of the modulation frequency, i.e., $f_p = P \times f_m$. This can be easily achieved in practice by slightly detuning the modulation frequency from its optimal harmonic mode-locking value, by a quantity corresponding to a fraction of the FSR, so that $f_m = (N + R/P)\mathrm{FSR}$, where R and P are integers having no common divisiors. In these conditions, only $P \times f_m$ and its harmonics match cavity resonance modes, whereas frequency components at all other multiples of f_m (including the spur at f_m itself) tend to vanish, and a pulse train at $f_p = P \times f_m$ is produced. Apart from this modulation frequency adjustment, RHML basically does not require any particular disposition of the set-up, which outlines the extreme versatility of this technique.

Through the use of RHML, repetition rate multiplications up to a factor $P = 22$ were achieved [2], and repetition rate values as high as 200 GHz were reached [3]. Unfortunately, an inherent drawback of this technique is the existence of a strong pulse-to-pulse amplitude fluctuation in the train [3], which corresponds in the spectrum to imperfectly suppressed components at f_m and its unwanted harmonics. Such an amplitude fluctuation is unacceptable for most applications. Hence, this intrinsic defect of RHML considerably reduces its practical interest in most cases. Nevertheless, it was recently demonstrated that, in the particular case $P = 2(R = 1)$, and if f_m is precisely tuned to a half-integer multiple of the FSR, the pulse-to-pulse amplitude fluctuation of the repetition-rate-doubled pulse train vanishes [4,5]. Therefore, and in spite of the modest twofold multiplication that is achieved, second-order RHML appears as the most attractive technique for applications.

Most applications employing high-speed picosecond pulse sources show extremely limited tolerance for the noise characteristics of the pulse train [6,9], whereas fibre lasers are very sensitive to external perturbations. For this reason, the measurement of the noises affecting these sources has long been a commonly addressed issue. Now, although it is usually observed that RHML enhances the sensitivity of fibre lasers to perturbations, the study of noises in this regime has received very few consideration so far. An important task thus consists in measuring accurately these noises, in order to investigate the processes underlying their formation, whose knowledge is likely to give hints for their reduction.

The measurement of the phase noise affecting the envelope of optical pulses in a train (or equivalently, the pulse timing jitter) has always benefited from a particular attention in the literature. Recent developments account for specific techniques relying on optical cross-correlation [10,11], time-interval analysis [12,13] and phase-encoded optical sampling [7]. On the other hand, fluctuations of the pulse intensity (i.e., amplitude noise) are sometimes characterised in a very natural way by envelope detecting, using a Shottky diode, the train of current pulses from a photodetector illuminated by the optical pulse train [6,8,9], or by measuring variations of the baseband (DC) component of this current pulse train [14].

The most popular techniques for characterising the noises of a pulse train are those that allow the measurement of both amplitude and phase noises. A famous example in this category is offered by the widespread spectral analysis technique, which was originally proposed by von der Linde in the mid-eighties [15]. In this technique, amplitude and phase noises are determined from the measurement of the noise skirts surrounding two harmonics in the radio-frequency spectrum of the detected pulse train. This was made possible by observing that, in each of these skirts, the phase

noise contribution scales as the square of the harmonic number, whereas the amplitude noise contribution is the same at all harmonics. Unfortunately, this assertion relies on several assumptions, like the smallness of amplitude and phase noises, and is no longer valid when high-order harmonics are considered [16].

There is an alternative technique that allows to measure both amplitude and phase noises of a pulse train. This technique relies on the homodyne downconversion of one harmonic of the pulse train detected by a photodetector. Its principle results from the observation that, in a sinusoidal carrier, small AM and PM modulations correspond, in first approximation, to in-phase and in-quadrature components, respectively [14]. We will now have a closer look at this technique. Obviously, if the detected pulse train shows up some amplitude noise $\varepsilon(T)$ and some phase noise $\phi(T)$, then its first harmonic $V_1(t,T)$ is modulated in amplitude by $\varepsilon(T)$, and in phase by $\phi(T)$, i.e.,

$$V_1(t,T) = V_0[1+\varepsilon(T)]\cos[2\pi f_p t - \phi(T)]. \quad (1)$$

Note that, in Eq. (1), ε and ϕ do not depend on t, but on T, which is defined as a coarse-grained time that evolves at the scale of many cavity roundtrips. This is valid if only low-frequency noises, which fluctuate very slowly at the scale of pulse duration or pulse train period, are considered. In order to determine in-phase and in-quadrature components of $V_1(t,T)$, which will yield $\varepsilon(T)$ and $\phi(T)$, $V_1(t,T)$ is mixed with a sinusoidal reference signal at the same frequency f_p (i.e., the pulse train repetition rate), either in phase or in quadrature. If we neglect the noise of the reference signal (assuming that a low-noise oscillator is used), after low-pass filtering, the output of the mixer is given by

$$V_{re}(T) = \frac{\alpha}{2} V_0 V_{ref}[1+\varepsilon(T)]\cos[\phi(T)] \quad (2)$$

for in-phase input signals, and

$$V_{im}(T) = \frac{\alpha}{2} V_0 V_{ref}[1+\varepsilon(T)]\sin[\phi(T)] \quad (3)$$

for in-quadrature input signals, where α is the mixer conversion constant and V_{ref} is the magnitude of the reference signal. Eqs. (2) and (3) show that $V_{re}(T)$ and $V_{im}(T)$ depend on both $\varepsilon(T)$ and $\phi(T)$. However, assuming that $\varepsilon(T)$ and $\phi(T) \ll 1$, we find that $V_{re}(T) \approx \alpha/2 V_0 V_{ref}[1+\varepsilon(T)]$ and $V_{im}(T) \approx \alpha/2 V_0 V_{ref}\phi(T)$ give good approximations of amplitude and phase fluctuations, respectively, in the time domain. Through the use of a spectrum analyser, these time-domain signals can be observed in the frequency domain, which is usually more convenient for their analysis.

The technique presented above is of very common practice mostly for phase noise measurement, and is called in this case the phase detector method [17]. In particular, when the reference oscillator used for in-quadrature detection is the generator that drives the actively mode-locked laser, this technique allows to measure the so-called residual phase noise of the pulse train, which is the phase noise from which the contribution of the mode locker, $\phi_{ml}(T)$, has been taken out [8,9,17–23]. Indeed, if the reference signal includes a substantial amount of phase noise $\phi_{ref}(T)$, then $\phi(T)$ has to be replaced by $\phi(T) - \phi_{ref}(T)$ in Eq. (3) (and in Eq. (2)). Now using again the small-noise approximation, we find that $V_{im}(T) \approx \alpha/2 V_0 V_{ref}[\phi(T) - \phi_{ref}(T)]$, so that $V_{im}(T)$ yields the residual phase noise $\phi(T) - \phi_{ml}(T)$ when the reference signal is taken from the mode locker. This procedure allowing to wipe away the effect of the mode locker is extremely useful, as this trivial source of phase noise usually brings the largest contribution to the pulse train phase noise [6,24,25], and obscures thereby the contributions of more discrete, although more fundamental physical processes. In particular, the measurement of residual phase noise can be used to determine the phase noise quantum limit of actively mode-locked laser systems [20,23].

As said before, the amplitude noise $\varepsilon(T)$ can be obtained from $V_{re}(T)$, which is measured at the output of the mixer when its input ports are fed with in-phase pulse train and reference signals. This of course results from small-noise approximation, as $V_{re}(T)$ also depends on $\phi(T)$, strictly speaking (see Eq. (2)). It is possible, however, to suppress $\phi(T)$ from the measurement of $\varepsilon(T)$ in a very simple way, by using the first harmonic of the detected pulse train itself as the reference signal [19,26]. Indeed, by in-phase mixing $V_1(t,T)$ with itself, the phase noise contribution in the output

signal cancels out, whereas the sensitivity of $V_{\mathrm{re}}(T)$ to amplitude noise is enhanced. More precisely, Eq. (2) then becomes (neglecting the term in ε^2):

$$V_{re}(T) = \frac{\alpha}{2} V_0^2 [1 + 2\varepsilon(T)]. \tag{4}$$

Unfortunately, things are not that simple in the case of phase noise measurement. Indeed, there is no way to isolate completely $\phi(T)$ from $\varepsilon(T)$ by the measurement of $V_{\mathrm{im}}(T)$ through in-quadrature detection of $V_1(t,T)$ (see Eq. (3)). Therefore, care must always be taken that $\varepsilon(T)$ be small enough for the approximation $V_{\mathrm{im}}(T) \propto \phi(T)$ to remain valid. In practice, it is usual to observe that the spectrum of the phase noise obtained this way includes some features that are recognised as a residual signature of amplitude noise [6,23].

The imperfect uncoupling between amplitude and phase noises operated by the homodyne downconversion technique arises from the fact that $\varepsilon(T)[\phi(T)]$ is derived from the sole quantity $V_{\mathrm{re}}(T)[V_{\mathrm{im}}(T)]$, which requires small-noise approximation. If now $V_{\mathrm{re}}(T)$ and $V_{\mathrm{im}}(T)$ are measured at the same time (i.e., over the same time interval), through simultaneous in-phase and in-quadrature detection of the input signal (this requires of course a second mixer), then $\varepsilon(T)$ and $\phi(T)$ can be obtained without small-noise approximation. Indeed, using Eqs. (2) and (3), we find that

$$\phi(T) = \tan^{-1}\left[\frac{V_{\mathrm{im}}(T)}{V_{\mathrm{re}}(T)}\right], \tag{5}$$

and

$$\varepsilon(T) = \frac{\sqrt{V_{\mathrm{re}}^2(T) + V_{\mathrm{im}}^2(T)} - \frac{\alpha}{2} V_0 V_{\mathrm{ref}}}{\frac{\alpha}{2} V_0 V_{\mathrm{ref}}}. \tag{6}$$

Like previously, these noises are more conveniently analysed in the frequency domain, through the calculation of their power spectral densities (PSDs) $S_\varepsilon(f)$ and $S_\phi(f)$, respectively. In addition to this, as $\varepsilon(T)$ and $\phi(T)$ cover the same time interval, it is possible to compute the cross-spectral density (XSD) between these two noises, $S_{\varepsilon\phi}(f)$. This quantity, which is not available using classical noise measurement techniques, is extremely useful to assess the degree of correlation between the noises in different frequency ranges. The technique presented here allows to infer more precise information about amplitude and phase noises than the conventional homodyne downconversion technique, and thus constitutes a substantial improvement of the latter. This technique is known as the time-domain demodulation technique, and was first used by Tsuchida to characterise the noises of passively and hybridly mode-locked lasers [13,27,28].

In this paper, we investigate, both theoretically and experimentally, the influence of environmentally induced cavity length variations on the noises affecting an optical pulse train generated by a fibre laser in the second-order RHML regime. In Section 2, we determine theoretically this influence, on the basis of a simple although instructive model that was recently proposed. In Section 3, we show how the signals obtained through time-domain demodulation of the detected pulse train must be interpreted in the particular case of second-order RHML. A comparison is then performed in Section 4 between theoretically predicted and experimentally measured energy and phase fluctuations that take place in the pulse train under the effect of a voltage-controlled cavity length variation. In Section 5, we use the time-domain demodulation technique to characterise experimentally energy and phase noises affecting the pulse train from a fibre laser in normal second-order RHML operating conditions. Finally, general conclusions are drawn in Section 6.

2. Effect of environmental perturbations on a repetition-rate-doubled pulse train

In this section, we study theoretically the effect of a change in the cavity length by using a recently proposed model of pulse train generation in the second-order RHML regime [4,5]. Although this model, based on the self-consistency of the pulses after two consecutive round-trips in the cavity, does not take into account dispersive and nonlinear effects, we believe that it will be helpful to understand the mechanisms through which cavity length variations result in the energy and phase fluctuations that will be measured in the detected pulse train.

In the case of a harmonically mode-locked laser, a pulse train is generated at a repetition rate

that is equal to the modulation frequency, which is ideally chosen to be an integer multiple of the cavity fundamental frequency, or FSR. As a consequence, every modulation period, only one pulse circulating in the cavity crosses the modulator, at the time when its transmittance is maximal. In contrast, through second-order RHML, it becomes possible to generate a pulse train whose repetition rate is twice the modulation frequency. In this case, two pulses in the cavity cross the modulator every modulation period. As a consequence, both pulses cannot be clocked at the maxima of transmittance (more generally, for any order of RHML, it is impossible that all pulses be clocked at these maxima). The aforementioned model was used to accurately reveal the pulse timing relationship in the second-order RHML regime. It showed in particular that, if the modulation frequency is perfectly tuned to a half-integer multiple of the FSR (case of optimal second-order RHML), the intracavity pulses cross the modulator at times corresponding roughly to the quadrature points, which are located half way between maximal and minimal transmittance (see curve T_A in Fig. 1). We note that there are two quadrature points within each modulation period. This result shows in particular that pulses do not alternate at the maxima and minima of the periodic transmittance, contrary to a formerly commonly held idea.

At first glance, it might seem surprising that pulses be able to maintain themselves at times where the slope of the transmittance curve is maximal (instead of zero in the case of harmonic mode locking). Indeed, round-trip after round-trip, this loss gradient across the pulses should tend to shift their positions progressively towards maximal transmission. In order to raise this incoherence, one has to consider that, in second-order RHML, the cavity round-trip time corresponds to a half-integer multiple of the modulation period. As a consequence, after each round-trip, the transmittance is shifted by half a period (curve T_B in Fig. 1), so that pulses once located at the rising edge will be clocked at the falling edge after one round-trip, and conversely. At the quadrature points, the slopes of the transmittance and of its π-shifted counterpart are equal and opposite, so that after two round-trips, their cumulated effect on the pulses position

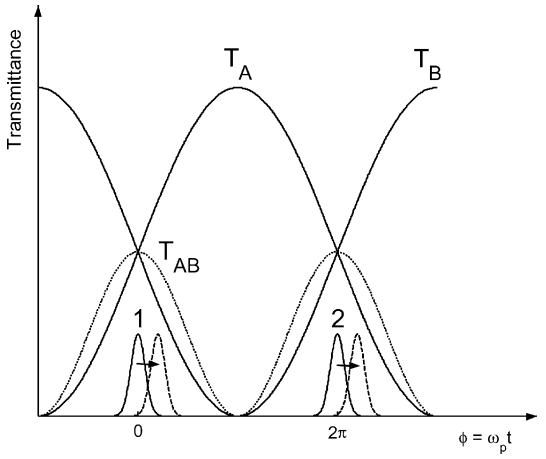

Fig. 1. Temporal evolution of the transmittance in an actively mode-locked fibre laser in the second-order RHML regime. This transmittance alternates between T_A and T_B (the π-shifted version of T_A) during successive round-trips. When the cavity length is properly tuned, pulses 1 and 2 (solid lines) are clocked approximately at the quadrature points of the transmittance (T_A or T_B). These positions correspond to the maxima of the effective transmittance $T_{AB} = T_A \times T_B$. If the laser length is slightly increased from its optimal value, the pulses undergo a positive phase shift (arrows), and stabilise at a position where the slope of the effective transmittance is negative (dashed lines). $\omega_p = 2\pi f_p$ and f_p is the pulse train repetition rate (twice the modulation frequency f_m).

cancels out, and the pulses can maintain themselves at these positions in regime. Moreover, as it appears that a cycle in the laser is not made of one, but of two round-trips in the second-order RHML regime, one should consider the transmittance curve that results of two consecutive round-trips in order to determine the pulse positions in regime. This curve, which is invariant from cycle to cycle, is obtained by making the product of two consecutive one-round-trip transmittances, and is a periodic function of time that oscillates at twice the modulation frequency (curve T_{AB} in Fig. 1). We observe that the maxima of this resulting transmittance correspond to the quadrature points of the one-round-trip transmittance curves. Hence, in the second-order RHML regime as well as in the usual harmonic mode locking regime, pulses are clocked at the maxima of the transmittance experienced by the pulses during each cycle.

Up to now, we considered that the round-trip time, fixed by the cavity length, equals precisely a

half-integer multiple of the modulation period or, in other words, that the cycle time is an (odd) integer multiple of this period. If now the cavity length is slightly detuned from its optimal value, the time required by the pulses to run one cycle is changed. Therefore, cycle after cycle, the pulses progressively walk off from the modulation maxima. If it is not compensated, this walk-off will result in the loss of mode locking. However, for very small values of the detuning, this walk-off is eventually equilibrated by a pushing or pulling effect that is due to the slope of the transmittance curve T_{AB} off its maximum. When the slope becomes sufficient, the pulses position is thus stabilised with respect to the transmittance curve, and a regime is reached (see Fig. 1 in the case of a positive cavity length detuning). This adaptation of the pulses phase consequent to a small detuning is not a property specific to second-order RHML, as it also occurs in the harmonic mode-locking regime [29].

The model presented in [4,5] can be used to refine this intuitive description of second-order RHML. This model allows in particular to determine the position of the pulses (in regime) for any value of cavity length detuning. Fig. 2 shows the phases ϕ_1 and ϕ_2 (modulo 2π) of two consecutive pulses, together with their average value ϕ_0, as functions of the relative cavity length detuning. These curves were calculated using parameters of the experiments described in Sections 4 and 5. As expected from the above discussion, the pulses positions stabilise for any value of small cavity length detuning, and their phases grow monotonously with detuning. Both curves do not superimpose, however: this means that the phase shifts of pulses 1 and 2 consecutive to the same detuning are not rigorously identical. This asymmetry between pulses 1 and 2 seems to be in contradiction with the periodicity of the resulting modulation T_{AB}, which is equal to that of the pulse train, so that the action of T_{AB} on both pulses is identical (see Fig. 1). Even at zero detuning, the pulses phases are still slightly different, and their positions do not match exactly the maxima of T_{AB}, i.e., the quadrature points of T_A and T_B, where $\phi = 0$ (see Fig. 2, inset). This can be understood by noticing that the effective frequency-doubled transmittance T_{AB} results from the product of two transmittances that do not have the periodicity of the pulse train (thus affecting differently pulses 1 and 2), and whose actions on each pulse are not simultaneous, but consecutive. In particular, round-trip after round-trip, the slope of the transmittance (T_A or T_B) experienced by the pulses is alternately positive and negative, and triggers an alternation in the position of each pulse between two slightly different values. For example, if detuning is zero, the pulses oscillate between two positions equidistant from the quadrature points of the one-round-trip transmittance. In Fig. 2, we considered that the last transmittance experienced by pulses 1 and 2 prior to detection was T_A. Given the respective signs of the slope of T_A about pulses 1 and 2, it comes that $\phi_1(0)$ is slightly positive, whereas $\phi_2(0)$ is slightly negative (the average phase $\phi_0(0) = 0$, for reasons of symmetry). Fig. 2

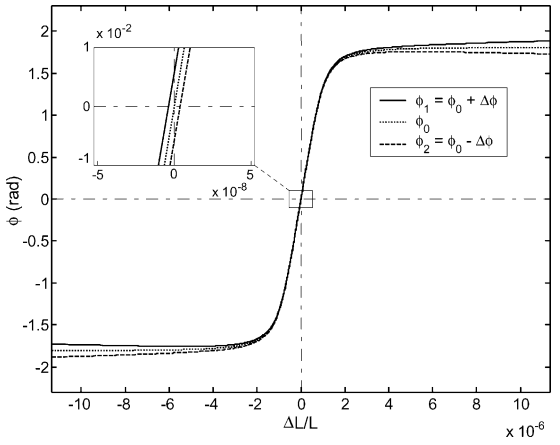

Fig. 2. Evolution of the phases ϕ_1 and ϕ_2 (modulo 2π) of two consecutive pulses, and of their average value ϕ_0, as functions of the relative cavity length detuning in the second-order RHML regime. These curves were obtained using the model described in [4,5], with parameters measured from the experimental setup described in Section 4. The electric-field transmittance of the Mach–Zehnder modulator writes as $T_A(t) = \sin[\psi_0 + \pi R \sin(\phi/2)]$, where $\phi = \omega_p t = 2\omega_m t$, ψ_0 is the phase factor, and $R = V_M/V_\pi$ where V_M is the amplitude of the modulation voltage and V_π is the half-wave voltage of the modulator. We measured that $\psi_0 = 0.29\pi$ and $R = 0.19$. In addition, we considered a modulation frequency $f_m = 1.297$ GHz, and we measured the FSR = 1.437 MHz, the 3-dB bandwidth of the tuneable optical bandpass filter $\Delta\lambda = 2.2$ nm, and $k_s = 1$ (k_s is a parameter fixed by the finesse of the filter, which is assumed to be a Fabry–Perot in the model).

also shows that the pulse-to-pulse phase difference, $\phi_1 - \phi_2 = 2\Delta\phi$, is not constant versus detuning. It has to be noted, however, that $\Delta\phi$ remains very small compared to ϕ_0, and a slight divergence between the curves in Fig. 2 appears only for rather large values of detuning. In summary, when cavity length detuning takes place in a laser operated in the second-order RHML regime, not only the average phase ϕ_0 of the pulses is modified, but also the pulse-to-pulse phase difference, $2\Delta\phi$. The latter never strictly vanishes, even for zero detuning.

The model also allows to infer information about the energy of the pulses. It predicts in particular that an energy difference between pulses 1 and 2 appears when the cavity length is detuned from its optimal value. Indeed, in the presence of some detuning, the average phase ϕ_0 is no longer zero, so that the positions of pulses 1 and 2 are shifted in the same direction with respect to their zero-detuning positions. As a consequence, the loss undergone through the modulator is different for both pulses. Let us consider the case of a positive detuning (Fig. 1). This positive detuning generates a positive phase shift of both pulses, so that the transmittance is either higher (T_A) or lower (T_B) for pulse 1 than for pulse 2. As a consequence, round-trip after round-trip, the energy of pulse 1 is alternately higher and lower than that of pulse 2, but always different (whereas the average energies of these two pulses over two consecutive round-trips are always equal). The modules of this difference increases with detuning. For zero detuning, however, both pulses experience the same loss through either T_A or T_B, and this energy difference vanishes.

In addition to this pulse-to-pulse energy difference, the average energy of the pulses (or equivalently, the average pulse train power) also varies with detuning. Indeed, for increasing detuning, the global transmittance experienced by the pulses after two consecutive round-trips (T_{AB}) diminishes, so that the overall intracavity loss, and thereby the average power of the generated pulse train, vary with detuning (see Section 4). In summary, when cavity length detuning takes place in a laser operating in second-order RHML regime, both the average energy of the pulses and their pulse-to-pulse energy difference are modified. Note that the model predicts a substantial increase in the durations of the pulses when detuning appears. As a consequence, the pulse energy fluctuations that we consider here account for fluctuations of both the amplitude and the duration of the pulses.

3. Effect of environmental perturbations on the pulse train harmonics

In the previous section, we have seen that, in the second-order RHML regime, cavity length detuning affects the average energy and phase of the pulses, as well as the pulse-to-pulse energy and phase differences. As a consequence, it is important to understand which impact these four fluctuations affecting the repetition-rate-doubled pulse train have on the amplitude and on the phase of its harmonics, which are the quantities that will be accessed using the time-domain demodulation technique. We consider that variations of cavity length, and thus energy and phase fluctuations are very slow compared to the pulse train period, so

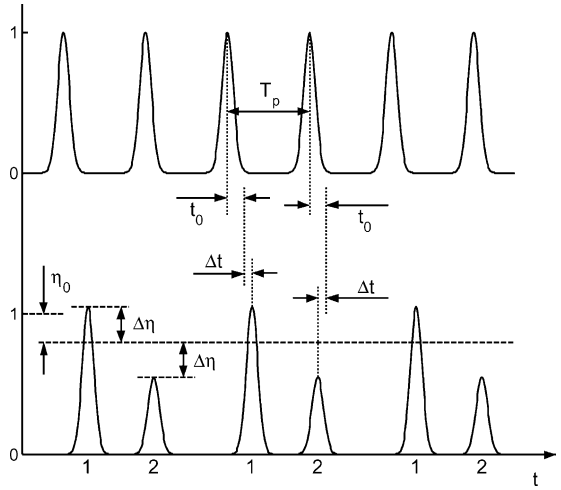

Fig. 3. Deviation from the ideal picture (upper trace) of a repetition-rate-doubled pulse train obtained by second-order RHML of a fibre laser in the presence of cavity length detuning. For the simplicity of this symbolic representation, fluctuations of the pulses amplitude are labeled as fluctuations of their energy (η_0 and $\Delta\eta$). In reality, however, energy fluctuations also include a contribution from the fluctuations of the pulse width (or duration).

that they can be described as functions of the coarse-grained time T. An ideal train of identical and regularly spaced pulses at the repetition rate $f_p = 2f_m$ (Fig. 3, up) can be expanded in Fourier series as

$$p(t) = \sum_{n=-\infty}^{+\infty} h\left(\frac{t - nT_p}{q}\right) = \sum_{k=0}^{+\infty} A_k \cos\left(k\omega_p t\right),$$

$$\text{with } A_0 = \frac{1}{T_p} qH(0) \text{ and } A_k = \frac{2}{T_p} qH(kq\omega_p) \text{ for } k > 0, \tag{7}$$

where $h(\zeta)$ is the temporal profile of the pulse power, q is the pulse duration, $T_p = 1/f_p$ is the pulse train period, $\omega_p = 2\pi f_p$ and $H(\Omega)$ is the Fourier transform of $h(\zeta)$. Now, including in Eq. (7) the four perturbations introduced above (Fig. 3, down), we obtain

$$p(t) = p_1(t) + p_2(t) = \sum_{n=-\infty}^{+\infty} (1+\alpha_1) h\left(\frac{t - 2nT_p - t_0 - \Delta t}{q(1+\tau_1)}\right) + \sum_{n=-\infty}^{+\infty} (1+\alpha_2) h\left(\frac{t - (2n+1)T_p - t_0 + \Delta t}{q(1+\tau_2)}\right), \tag{8}$$

where α_1 and α_2 are the relative amplitude fluctuations of pulses of type 1 and 2, respectively, τ_1 and τ_2 are the relative fluctuations of their duration, $t_0 = \phi_0/\omega_p$ is the average timing fluctuation of both types of pulses, and $\Delta t = \Delta\phi/\omega_p$ is half the pulse-to-pulse period variation. In order to simplify notation, the dependence of all these parameters on the coarse-grained time T was not indicated in Eq. (8). Eq. (8) expresses that $p(t)$ is not a perfect repetition-rate-doubled pulse train, but instead a superposition of two temporally shifted pulse trains each having the repetition rate f_m. In the general case of non-zero cavity length detuning, the amplitudes, durations and phases of the pulses are different between these two pulse trains. When detuning vanishes, the amplitudes and durations of the pulses in both trains become equal, although a slight phase difference remains ($\Delta t \neq 0$), so that the time separating consecutive pulses is never strictly equal to the (average) pulse train period T_p. As a consequence, strictly speaking, an optical pulse train obtained through second-order RHML can never be written as Eq. (7). Using Eq. (7), assuming small fluctuations and considering that $q\omega_p \ll 1$ so that $H[kq(1+\tau_i)\omega_p] \approx H(0) \approx H(kq\omega_p)$, we find, after some calculation,

$$\begin{aligned} p(t) = {} & (1+\eta_0) \sum_{k=0}^{+\infty} A_k \cos(2k\omega_m \Delta t) \\ & \times \cos[2k\omega_m (t - t_0)] + \Delta\eta \sum_{k=0}^{+\infty} A_k \\ & \times \sin(2k\omega_m \Delta t) \sin[2k\omega_m (t - t_0)] \\ & + 2(1+\eta_0) \sum_{k=0}^{+\infty} B_{2k+1} \sin((2k+1)\omega_m \Delta t) \\ & \times \sin[(2k+1)\omega_m (t - t_0)] \\ & + 2\Delta\eta \sum_{k=0}^{+\infty} B_{2k+1} \cos((2k+1)\omega_m \Delta t) \\ & \times \cos[(2k+1)\omega_m (t - t_0)], \end{aligned}$$

$$\text{with } B_k = \frac{2}{2T_p} qH(kq\omega_m), \tag{9}$$

where $\eta_0 = (\eta_1 + \eta_2)/2 = (\alpha_1 + \tau_1 + \alpha_2 + \tau_2)/2$ is the average pulse energy fluctuation, and $\Delta\eta = (\eta_1 - \eta_2)/2 = (\alpha_1 + \tau_1 - \alpha_2 - \tau_2)/2$ is half the pulse-to-pulse energy fluctuation. Again, the dependence on T of the fluctuations was omitted in the equation. Eq. (9) shows that pulse-to-pulse fluctuations Δt and $\Delta\eta$ generate odd-order harmonics of the modulation frequency $\omega_m = \omega_p/2$, which correspond to the last two terms in the right-hand-side of the equation. The sum of these odd-order components never vanish, but is minimal when detuning is zero (in this case, $\Delta\eta = 0$ and Δt is minimal) [4,5]. On the other hand, it appears from Eq. (9) that all fluctuations, t_0, Δt, η_0 and $\Delta\eta$ affect even-order harmonics of ω_m, both in amplitude and in phase, in a very intricate way, so that it is impossible in general to determine any of these fluctuations from time-domain demodulation of one of these harmonics. This difficulty can be overcome, however, by considering only small fluctuations (in particular, Δt is extremely small), so that we can neglect second-order terms. Let us

consider in particular the first harmonic of $\omega_p = 2\omega_m$, corresponding to the first two terms of the right-hand-side in Eq. (9), for $k = 1$. Expanding in Taylor series the cosine and the sine functions, and keeping only first-order terms in the small fluctuations, we readily obtain

$$h_1(t,T) \approx A_1[1+\eta_0(T)]\cos\{\omega_p[t-t_0(T)]\}. \quad (10)$$

Comparing Eq. (10) with Eq. (1), we observe that applying the time-domain demodulation technique to the first harmonic (at ω_p) of the repetition-rate-doubled pulse train yields the average pulse energy fluctuation $\eta_0(T)$ and the average phase fluctuation $\phi_0(T) = \omega_p t_0(T)$. In summary, looking at the spectrum of a pulse train generated through second-order RHML of a fibre laser subject to cavity length fluctuations, we can say in first approximation that even-order harmonics of the modulation frequency contain information about the average fluctuations of the pulses, whereas odd-order harmonics are the signature of pulse-to-pulse fluctuations.

4. Comparison of theory and experiment

In Section 2, we have seen that, using the model proposed in [4,5], it is possible to predict the characteristics of a pulse train generated by a fibre laser in second-order RHML regime, and in particular the average phase ϕ_0 and energy η_0 of the pulses, for any given value of the cavity length detuning. On the other hand, we demonstrated in Section 3 that ϕ_0 and η_0 can be determined through time-domain demodulation of the first harmonic of the repetition-rate-doubled pulse train. In this section, we compare the evolutions of η_0 and ϕ_0 that are obtained theoretically on the basis of the aforementioned model, and experimentally through time-domain demodulation, for the same temporal evolution of the detuning.

In order to control the cavity length detuning, which will drive phase and energy fluctuations, we consider that a sinusoidal dithering at 10 Hz is imposed to the cavity length. We assume that the magnitude of this dithering is significantly larger than that resulting of environmental perturbations, so that the latter can be neglected. As the 10-Hz dithering is extremely slow at the scale of mode-locking dynamics (~MHz), we may consider that a regime is reached for each instantaneous value of the detuning. Hence, knowing the bias and the magnitude of the periodic dithering, we can compute, using Fig. 2, the temporal evolution (versus T) of the pulses phase. This dithering is thus responsible for a periodic phase fluctuation of the pulses. Fig. 4 shows the evolution of the phases of pulses 1 and 2, as well as that of the average phase ϕ_0, when a 10-Hz dithering is applied. The one-round-trip electric field transmittance $T_A(\phi)$, calculated for parameters of the experiment (see legend of Fig. 2), is also represented, in correspondence with these curves. In Fig. 4(a), the detuning bias is zero, whereas in Figs. 4(b) and (c), it is slightly different from zero (being, respectively, positive and negative), and is equal to half the amplitude of the periodic detuning. The phases ϕ_0, ϕ_1 and ϕ_2 oscillate at the same frequency as the sinusoidal dithering, although the curves that are obtained are not pure sine waves, due to the saturation observed in Fig. 2 for large values of detuning.

The curves $M_1(T)$ and $M_2(T)$ in Fig. 4 represent the electric-field transmittance as a function of T for pulses 1 and 2, resulting from the oscillation of their positions on the rising and falling edges of the transfer function T_A, respectively. We have seen in Section 2 that, during successive round-trips, the position of each pulse alternates between the rising and falling edges of the transmittance. Therefore, for each value of the time T, $\phi_1(T)$ and $\phi_2(T)$ represent the positions occupied by every pulse in the train for two consecutive passes through the modulator. At these two positions, the values taken by the transmittance T_A are generally different, as shown by $M_1(T)$ and $M_2(T)$. Now, because of the large fluorescence time of erbium in silica (~10 ms), which is much larger than the round-trip time in the cavity, gain saturates at a value fixed by the average intracavity loss, which is proportional to the average loss through the modulator. The average intracavity power (or equivalently, the average output power), which is fixed by this value of the gain, is thus related to the average loss, or to its inverse, the average transmittance, of the modulator. Considering only small fluctuations, we may

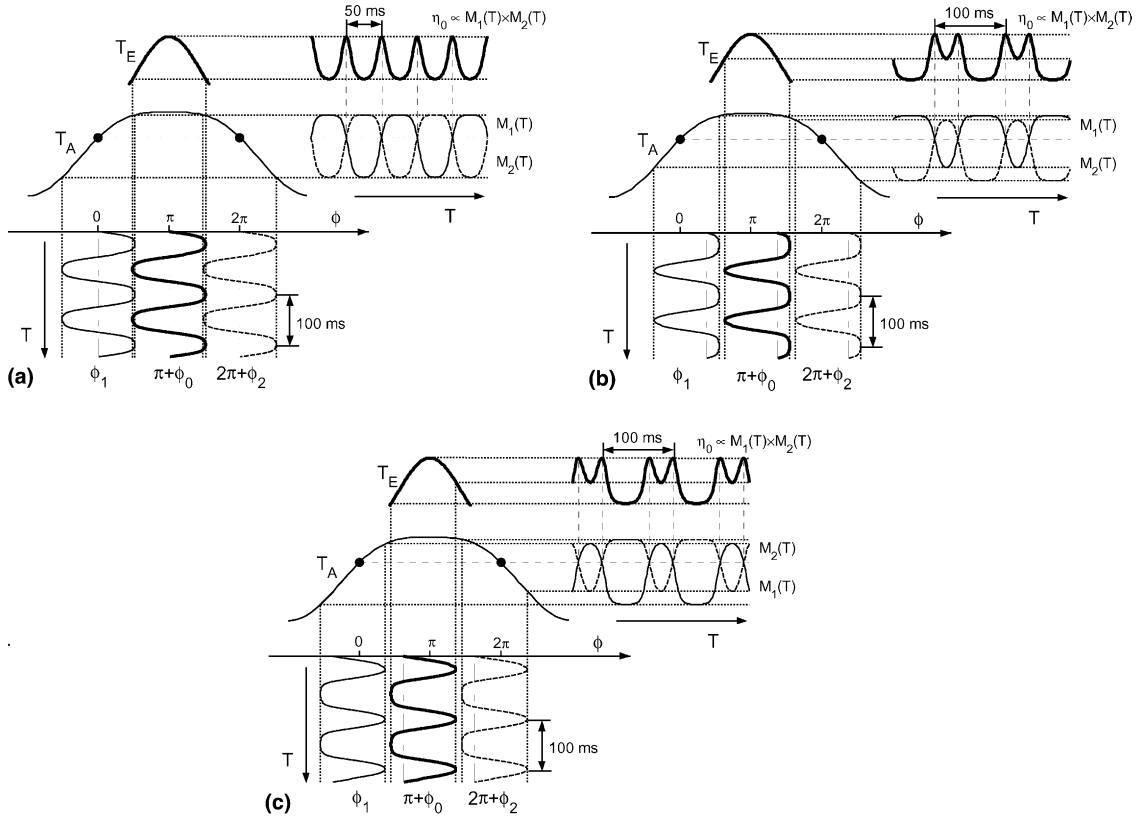

Fig. 4. Periodic variation of the pulses position and energy consecutive to a 10-Hz cavity length dithering for a fibre laser operated in the second-order RHML regime. The detuning bias is $\Delta L/L = 0$ (a), 8.15×10^{-7} (b), and -8.15×10^{-7} (c), and the amplitude of the periodic detuning is set to $\Delta L/L = 1.63 \times 10^{-6}$ in all cases. The one-round-trip electric field transmittance $T_A = \sin[\psi_0 + \pi R \sin(\phi/2)]$, and the values of all the parameters that were used in the model are given in the legend of Fig. 2. The filled circles in curve T_A for $\phi = 0$ and $\phi = 2\pi$ indicate the positions of the quadrature points. The phases ϕ_1 and ϕ_2 of the pulses, as well as their average value ϕ_0, oscillate around a value corresponding to the detuning bias (dashed-dotted vertical lines). They are presented as functions of a coarse-grained time T, which describes phenomena that evolve slowly at the scale of the cavity round-trip time. Through T_A, phase fluctuations induce the transmittance fluctuations $M_1(T) = T_A[\phi_1(T)]$ and $M_2(T) = T_A[\phi_2(T) + 2\pi]$, which affect pulses 1 and 2, respectively. These fluctuations are responsible for a fluctuation of the average pulse energy $\eta_0(T) \propto M_1(T) \times M_2(T)$. In practice, it is more convenient to consider that $\eta_0(T)$ results from the fluctuation of $\phi_0(T)$ through an effective transmittance characteristic $T_E(\phi)$.

suppose that the average power of the generated pulse train evolves linearly with the average intensity transmittance. From the above, it comes that the temporal evolution of this intensity transmittance, averaged over two consecutive round-trips, is the product of the individual electric-field transmittances $M_1(T)$ and $M_2(T)$. This average intensity transmittance is materialised in Figs. 4(a)–(c). This function gives thus a picture of the evolution of the average pulse train power or, equivalently, of the average pulse energy, η_0, as a function of time T. As each value of the average phase ϕ_0 corresponds to defined values of ϕ_1 and ϕ_2 (see Fig. 2), there is a one-to-one correspondence between ϕ_0 and the average intensity transmittance (or η_0). As a consequence, it is possible to construct an effective transfer characteristic $\eta_0 = T_E(\phi_0)$, by joining all points whose coordinates are given by a value of ϕ_0 and the corresponding value of η_0. This effective transmittance, which is represented in Fig. 4, will help us to understand the relation between phase and energy fluctuations when second-order RHML is employed.

As it appears from Fig. 4, T_E shows a maximum at $\phi_0 = 0$ (i.e., at zero detuning), and is symmetric about this point. Therefore, when the detuning bias is equal to zero (Fig. 4(a)), η_0 oscillates at twice the dithering frequency, i.e., at 20 Hz. This oscillation occurs at 10 Hz, however, when a non-zero bias is present (Figs. 4(b) and (c)). If this bias is positive (Fig. 4(b)), the slope of T_E is negative, so that η_0 is π-shifted with respect to ϕ_0. In contrast, both curves are in phase in the case of a negative bias, due to the positive slope of the transfer characteristic in this region (Fig. 4(c)). In summary, the model predicts that, when an actively mode-locked fibre laser is operated in the second-order RHML regime and undergoes cavity length fluctuations, the action of the intracavity amplitude modulator is responsible for a strong correlation between the average energy and phase fluctuations of the generated pulse train. Qualitatively, this happens in the same way as in the case of harmonic mode locking [30].

In our experiment, we used an erbium-doped fibre laser in a sigma configuration (Fig. 5). Such a laser associates a unidirectional polarisation-maintaining ring (right on Fig. 5) and a double-pass, non-polarisation-maintaining branch, which is ended by a Faraday mirror (left) [31]. This structure benefits from the advantages of a polarisation-maintaining ring laser, while maintaining the possibility to insert non-polarisation-maintaining components in the structure. The effective length of the laser was about 143 m (corresponding to a FSR of 1.437 MHz). A 9.7-m erbium-doped fibre pumped by a 980-nm laser diode (150 mW maximal power) was used as the gain medium. To be consistent with the model, non-linear effects were minimised through the use of a moderate 50-mW pump power. Also, in order to compensate for the anomalous intracavity dispersion, a 8-m piece of dispersion compensating fibre ($D \approx -80$ ps/nm/km at 1530 nm) was inserted in the non-polarisation-maintaining branch of the

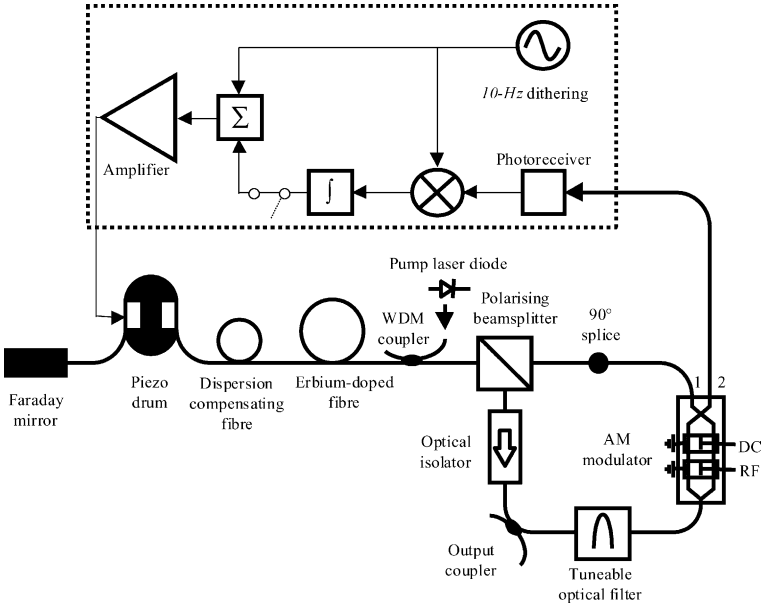

Fig. 5. Actively mode-locked erbium-doped fibre sigma laser with cavity length stabilisation scheme (dashed frame in the figure). The latter is based on the minimisation of the average interpulse noise that is measured at output 2 of the dual-output Mach–Zehnder amplitude modulator [32]. The correction voltage, together with a small 10-Hz sinusoidal voltage, is applied to a piezo drum on which a section of fibre is wound, thus adjusting the cavity length proportionally. This electronic feedback loop can be operated in both harmonic and second-order RHML regimes [33]. The 10-Hz dithering signal, which is normally used in the feedback loop to determine the sign of the correction voltage to be applied, is also used, in our experiments, when the feedback loop is turned off (in this case, the switch after the integrator is opened).

laser. Through the measurement of the dependence of the optimal modulation frequency on the operational wavelength (fixed by the central frequency of the tuneable optical filter), the total intracavity dispersion was estimated to be about −0.07 ps/nm at 1530 nm. In an attempt to reduce roughly environmental perturbations, the laser was placed in a foam plastic box. The modulation frequency was set to 1.297 GHz, i.e., 902.5 times the FSR, resulting in the generation of a 2.594-GHz optical pulse train. The average optical intracavity power was estimated to be 5–10 mW at the output coupler. From a background-free autocorrelation measurement, the pulse duration was determined to be 23 ps, a value that is very close to the theoretical value of 22.6 ps obtained by the model in the absence of cavity length detuning. Using an optical spectrum analyser, the optical bandwidth was measured to be about 0.15 nm. The slightly normal intracavity dispersion ensured the generation of gaussian-like pulses, as it was confirmed by a time-bandwidth product of 0.44, which corresponds to transform-limited gaussian pulses.

In this experiment, the cavity length stabilising feedback loop described in Fig. 5 was not used, except that a 10-Hz sinusoidal voltage was applied to the piezo drum, so as to generate a sinusoidal length dithering at this frequency. The magnitude of the voltage oscillation was set high enough so as to make this forced dithering take over environmental perturbations. When the laser was placed in the foam plastic box, this resulted in a detuning amplitude of $\Delta L/L = 1.63 \times 10^{-6}$, which can be compared to the relative length variation caused by about 1 °C temperature change (this means that temperature varied by much less than 1 °C over our measurement time of a few dithering periods). The generated optical pulse train was detected at the laser output by a 25-GHz photo detector, and the photocurrent was fed into a vector signal analyser, or VSA (Agilent Technologies, model 89441A), which performed amplitude and phase demodulation of its first harmonic (at 2.594 GHz). The time series of η_0 and ϕ_0 were then readily obtained.

It has to be stressed that, for this experiment, a particular care was taken for the choice of the RF generator used to operate the laser in the second-order RHML regime. Indeed, in an actively mode-locked fibre laser, the phase noise of the RF generator used as mode locker is often the dominant source of the pulse train phase noise. In fact, in many cases, the PSD of the latter literally mimics that of the generator phase noise [6,25]. As a result, the effect of other potential noise sources, in particular cavity length fluctuations, is masked. In contrast, the mode locker only slightly affects the energy noise of the pulse train. Therefore, the mode locker is not likely to generate a significant correlation between energy and phase noises of the pulse train, contrary to cavity length fluctuations. Hence, in order to show evidence of the influence of cavity length variations, in particular through the observation of the aforementioned correlation, one must get rid of the mode locker phase noise. One solution is to use the mode locker signal as the reference in the double demodulation process (see Section 1). As this was not achievable in our practical implementation (using the VSA), we used a low-noise generator (Hewlett Packard, model 83732A) as the mode locker.

The curves of Fig. 6 show $\eta_0(T)$ and $\phi_0(T)$, which were determined both experimentally by time-domain demodulation, and theoretically using the model. From (a) to (e), the detuning amplitude $\Delta L/L = 1.63 \times 10^{-6}$ was kept constant, while its bias was varied between $-\Delta L/L$ and $\Delta L/L$. The amplitudes of the theoretical curves were adjusted so as to fit at best the experimental results. A good agreement is then observed between the curves. In the case of η_0 (Fig. 6(I)), this agreement confirms that the average energy fluctuations determined experimentally are proportional to the average transmittance predicted theoretically. In the case of ϕ_0, Fig. 6(II) shows that the phase fluctuation determined theoretically is proportional in each case to the experimental data, but the proportionality coefficient is substantially smaller than unity, which denotes a quantitative discrepancy between the model and experimental results. Similarly to [4,5], we attribute this discrepancy to the increasing error of the theoretical model with increasing modulation frequency detuning, and also to the fact that this

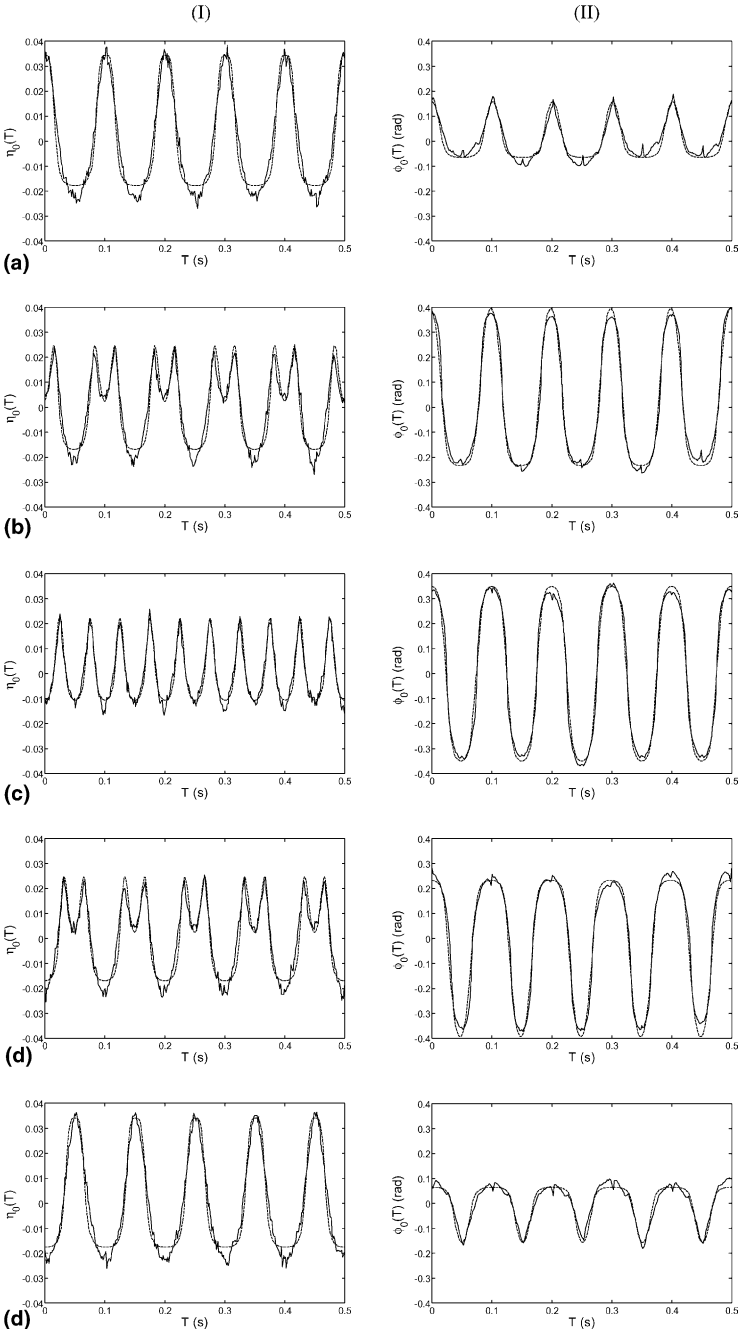

Fig. 6. Temporal evolution of the average pulse energy η_0(I) and of the average phase ϕ_0(II) of a pulse train generated by a fibre laser operated in the second-order RHML regime and whose length is modulated sinusoidally at 10 Hz. The values of the detuning bias that we considered are $\Delta L/L = -1.63 \times 10^{-6}$ (a), -8.15×10^{-7} (b), 0 (c), 8.15×10^{-7} (d) and 1.63×10^{-6} (e), for a detuning amplitude $\Delta L/L = 1.63 \times 10^{-6}$ in all cases. Solid lines are the experimental data, obtained by time-domain demodulation of the first harmonic of the detected pulse train, and dashed lines are theoretical curves, whose magnitudes have been fitted to experimental data, using the least square method.

model does not take into account intracavity dispersion (although its total value is close to zero, several sections of the laser show up a substantial amount of dispersion) and the Kerr non-linearity, which may have some influence on the pulse parameters. In spite of these limitations of the model, the qualitative agreement between theoretical and experimental data is very good, and the relation between phase and energy fluctuations due to the action of the modulator, which were predicted in Fig. 4, are clearly observed experimentally. In particular, when the detuning bias is zero, η_0 oscillates at 20 Hz, i.e., at twice the frequency of ϕ_0, which corresponds to the dithering frequency (Fig. 6(c)). In contrast, η_0 has a 10-Hz component when some bias appears. When this bias is negative, η_0 and ϕ_0 are in phase, whereas η_0 is π-shifted with respect to ϕ_0 in the case of a positive bias (compare Figs. 6(a) and (e), (b) and (d)).

5. Measurement of energy and phase noises

In this section, we measure, using the time-domain demodulation technique, energy and phase noises affecting a pulse train generated by the sigma laser in the second-order RHML regime, as well as the cross-correlation between these noises. The latter in particular will be very useful to assess the influence of environmentally induced cavity length fluctuations on the measured noises. For this study, the laser length was stabilised against long-term drifts through the implementation of the electronic feedback loop described in Fig. 5. In order to make environmental perturbations the dominant cause of cavity length fluctuations, the magnitude of the 10-Hz dithering was reduced to the minimal value that still ensures proper operation of the feedback loop. Like in the previous section, the laser was mode-locked at 1.297 GHz, resulting in the generation of a 2.594-GHz pulse train. The detected pulse train was fed into the VSA, which performed amplitude and phase demodulation of its first harmonic. The time series of average energy and phase noises, $\eta_0(T)$ and $\phi_0(T)$, respectively, were then retrieved from the analyser, and their PSDs, $S_{\eta 0}(f)$ and $S_{\phi 0}(f)$, as well as their XSD, $S_{\eta 0\phi 0}(f)$, were calculated using a FFT-based algorithm. We also measured the PSDs of amplitude and phase noises of the RF generator signal. These results are presented in Fig. 7.

In Figs. 7(a) and (b), it appears clearly that both energy and phase noises of the pulse train exceed those of the generator. This means that other physical processes than the generator noise perturb the pulse train more significantly. Contrary to the previous experiment (see Fig. 6), the influence of the 10-Hz dithering was not easy to identify from the direct examination of the time series $\eta_0(T)$ and $\phi_0(T)$, due to its very low magnitude. Its impact on amplitude and phase fluctuations can be observed, however, in the PSDs $S_{\eta 0}(f)$ and $S_{\phi 0}(f)$ (Figs. 7(a) and (b)), where spurs are visible at 10 Hz and its harmonics. Referring to the previous section, $S_{\eta 0}(f)$ should include spurs only at 20 Hz and its harmonics if the laser length was properly tuned. The existence in $S_{\eta 0}(f)$ of a spur at 10 Hz (and at its odd-order harmonics) indicates that, in spite of the use of a feedback loop to avoid cavity length drifts, the detuning bias is not precisely maintained to zero. In fact, this is not surprising if we consider that a change in the modulation frequency as small as a few tens of hertz from the optimal mode locking frequency (corresponding to a detuning $\Delta f_{\mathrm{m}}/f_{\mathrm{m}} \approx 10^{-8}$ only) suffices to generate a peak at 10 Hz in $S_{\eta 0}(f)$, as it was observed when the feedback loop was turned off (although the 10-Hz dithering was maintained). Such small detuning values lie in the range of the precision attained by the feedback loop. Note that, whereas the 10-Hz dithering voltage that is applied is a pure sine wave, a rather large number of harmonics of 10 Hz are visible in both $S_{\eta 0}(f)$ and $S_{\phi 0}(f)$. In the case of $S_{\phi 0}(f)$ (Fig. 7(b)), high-order harmonics may be due to the non-linear phase-versus-detuning characteristic (Fig. 2). They may also originate from some non-linearity in the voltage-extension characteristic of the piezo drum that adjusts the cavity length. In the case of $S_{\eta 0}(f)$ (Fig. 7(a)), the presence of high-order harmonics is mainly caused by the existence of such harmonics in $S_{\phi 0}(f)$, and by the non-linearity of the effective transfer characteristic $\eta_0 = T_{\mathrm{E}}(\phi_0)$ (Fig. 4). Finally, let us mention that the wide spur around 50 kHz in $S_{\eta 0}(f)$ (Fig. 7(a)) is the signature of relaxation oscillations.

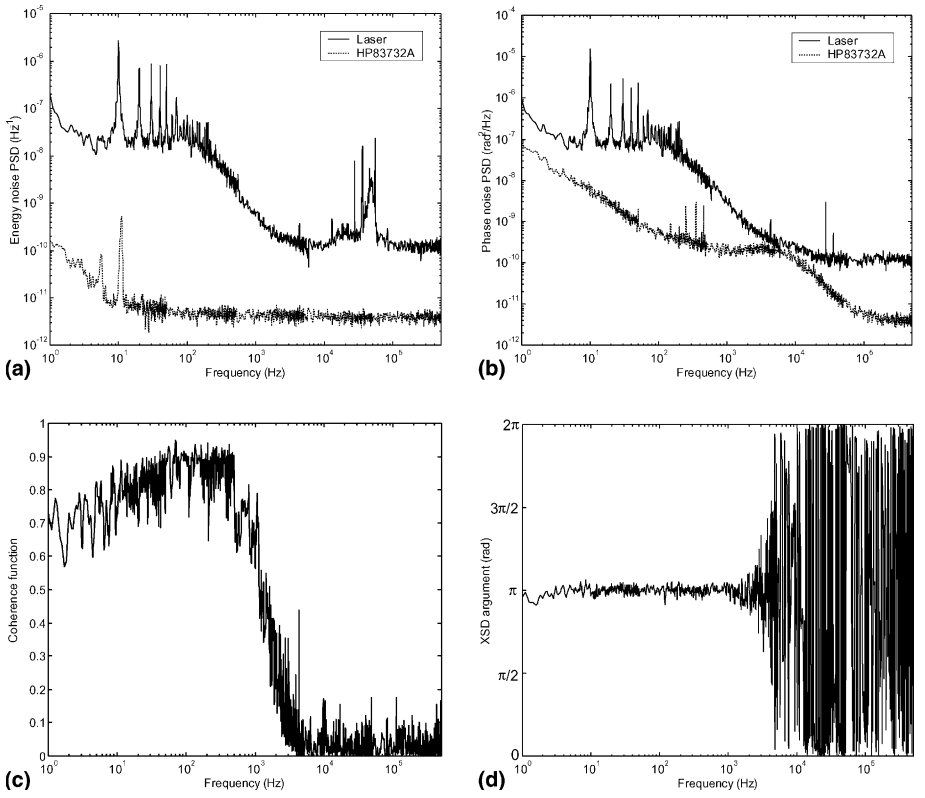

Fig. 7. PSD of η_0 (a), PSD of ϕ_0 (b), coherence function (c) and argument of the XSD $S_{\eta_0\phi_0}(f)$ (d) measured from a 2.594-GHz optical pulse train generated by the fibre sigma laser in the second-order RHML regime. The PSDs of amplitude (energy) and phase noises of the RF generator are also represented. Frequency span: 1 Hz–500 kHz. Each curve combines data from five measurements with different spans (50 Hz, 500 Hz, 5 kHz, 50 kHz and 500 kHz) and resolutions (0.1 Hz, 1 Hz, 10 Hz, 100 Hz and 1 kHz, respectively).

Fig. 7(c) shows the coherence function of η_0 and ϕ_0. The coherence function is the square modules of the XSD normalised to the PSDs, i.e.,

$$\gamma^2_{\eta_0\phi_0}(f) = \frac{|\, S_{\eta_0\phi_0}(f)\,|^2}{S_{\eta_0}(f)S_{\phi_0}(f)}. \tag{11}$$

This function is very useful, as it allows to quantify the degree of correlation at each frequency by values included between 0 and 1. From Fig. 7(c), it appears that a strong correlation exists between η_0 and ϕ_0 on a wide frequency range, which extends continuously up to several kHz, and is thus not restricted to a few discrete frequencies corresponding to the successive harmonics of the 10-Hz dithering. As the XSD $S_{\eta_0\phi_0}(f)$ is generally a complex quantity, additional information is provided by its argument, which is shown in Fig. 7(d). We observe that, in the frequency range where the coherence function shows up significant values (up to a few kHz), the argument of $S_{\eta_0\phi_0}(f)$ is approximately equal to π. Hence, $S_{\eta_0\phi_0}(f)$ is essentially real and negative at these frequencies. This is not a rule, however. Indeed, after making several noise measurements in the same conditions as for Fig. 7, we observed that, at frequencies where substantial coherence was measured, $S_{\eta_0\phi_0}(f)$ was real in all cases, but either positive ($\arg[S_{\eta_0\phi_0}(f)] = 0$) or negative ($\arg[S_{\eta_0\phi_0}(f)] = \pi$). In some cases, however, the coherence essentially vanished over the whole frequency range.

These observations can be explained very easily by considering the effect of environmental perturbations. Indeed, like the 10-Hz sinusoidal dithering that is applied to the piezo drum, environmental perturbations (temperature changes and mechanical vibrations) slightly modify the

cavity length (in a random way in the latter case). All these slow length variations induce fluctuations of the average phase ϕ_0 of the generated pulses (Fig. 2). These phase fluctuations are then turned into amplitude fluctuations, through the mediation of the effective transmittance characteristic, T_E (Fig. 4). In the PSDs $S_{\eta_0}(f)$ and $S_{\phi_0}(f)$ (Figs. 7(a) and (b)), the deterministic dithering appears as a series of spurs at 10 Hz and its harmonics, whereas the signature of random environmental perturbations is a continuous noise pattern that essentially rolls off for increasing frequencies, down to the measurement floor. Depending on the value of the detuning bias, the correlation between phase and energy noises as measured by the coherence function can be very different. First, if this bias is zero, then all phase fluctuations are frequency-doubled in the phase-to-energy-noise conversion process, because of the symmetry of the effective transmittance T_E (Fig. 4(a)). In particular, the 10-Hz phase variation yields a 20-Hz energy fluctuation of the pulses. As a consequence, the coherence function is close to zero at all frequencies. In contrast, if the detuning bias is slightly different from zero, phase fluctuations generate amplitude fluctuations at the same fundamental frequency. In particular, the 10-Hz phase variation yields a 10-Hz energy fluctuation of the pulses. In the case of a positive bias, the average position ϕ_0 of the pulses appears preferentially on the falling edge of the effective transmittance T_E (Fig. 4(b)). The slope of T_E being negative, $\eta_0(T)$ is π-shifted with respect to $\phi_0(T)$, and $S_{\eta_0\phi_0}(f)$ is negative. In contrast, if the bias is negative, the average pulse position appears on the rising edge of T_E (Fig. 4(c)). The slope being positive, $\eta_0(T)$ is in phase with $\phi_0(T)$, so that $S_{\eta_0\phi_0}(f)$ is positive. In summary, this section showed that random environmental perturbations are an important source of both energy and phase noises affecting a pulse train generated by a fibre laser in the second-order RHML regime.

6. Conclusions

In this paper, we studied both theoretically and experimentally the noise properties of an optical pulse train generated by an actively mode-locked erbium-doped fibre laser operated in the second-order rational harmonic mode locking regime. In particular, we investigated the effect of cavity length variations on the phase and energy fluctuations of the pulse train. Using a simple model of second-order rational harmonic mode locking, which was recently proposed, we showed that, when the cavity length changes, the average values of energy and phase, as well as the pulse-to-pulse energy and phase differences, fluctuate. Then we demonstrated that average energy and phase fluctuations can be measured simply by time-domain demodulation of the first harmonic of the detected pulse train. Through the application of a forced dithering to the cavity length, we were able to compare the average energy and phase fluctuations that were measured by time-domain demodulation with those predicted by the model. We observed a good qualitative agreement between theoretical and experimental results. This study showed in particular that average phase fluctuations are converted into energy fluctuations through the mediation of the modulator transmittance. The modalities of this conversion strongly depend on the value of the detuning bias. This mechanism of coupling between phase and energy noises of a repetition-rate-doubled pulse train obtained by rational harmonic mode locking is qualitatively very similar to the one that takes place in a harmonically mode-locked fibre laser. Finally, we measured, using the time-domain demodulation technique, the power spectral densities of the average energy and phase noises affecting the pulse train, as well as their cross-spectral density and coherence function. Our study showed that, when the phase noise of the RF generator is small enough, environmentally induced cavity length variations are the dominant source of both energy and phase noises of the pulse train. In many cases, we measured large coherence values, denoting the existence of a residual length detuning, which remains in spite of the implementation of an accurate stabilisation scheme. This demonstrates the extreme sensitivity of fibre lasers to environmental perturbations in the rational harmonic mode-locking regime.

Acknowledgements

This work is funded by the Inter-University Attraction Pole program (IAPV/18) of the Belgian Federal Office for Scientific, Technical and Cultural Affairs. The VSA was acquired thanks to the financial support of the Fonds de la Recherche Fondamentale Collective (F.R.F.C., convention 2.4578.00 F) of the Belgian Fund for Scientific Research (F.N.R.S.). The authors would also like to thank Ph. Emplit (Service d'Optique et d'Acoustique, Université Libre de Bruxelles) for providing the HP83732A.

References

[1] Z. Ahmed, N. Onodera, Electron. Lett. 32 (1996) 455.
[2] C. Wu, N.K. Dutta, IEEE J. Quantum Electron. 36 (2000) 145.
[3] E. Yoshida, M. Nakazawa, Electron. Lett. 32 (1996) 1370.
[4] R. Kiyan, O. Deparis, O. Pottiez, P. Mégret, M. Blondel, Opt. Lett. 25 (2000) 1439.
[5] R. Kiyan, O. Deparis, O. Pottiez, P. Megret, M. Blondel, Proc. SPIE 4354 (2000) 180.
[6] T.R. Clark, T.F. Carruthers, P.J. Matthews, I.N. Duling III, Electron. Lett. 35 (1999) 720.
[7] P.W. Juodawlkis, J.C. Twichell, J.L. Wasserman, G.E. Betts, R.C. Williamson, Opt. Lett. 26 (2001) 289.
[8] C.M. DePriest, A. Braun, J.H. Abeles, P.J. Delfyett, IEEE Photon Technol. Lett. 13 (2001) 1109.
[9] C.M. DePriest, T. Yilmaz, A. Braun, J. Abeles, P.J. Delfyett Jr., IEEE J. Quantum Electron. 38 (2002) 380.
[10] K. Tamura, M. Nakazawa, Opt. Lett. 23 (1998) 1360.
[11] L.A. Jiang, M.E. Grein, H.A. Haus, E.P. Ippen, IEEE J. Sel. Top. Quantum Electron. 7 (2001) 159.
[12] H. Tsuchida, Opt. Lett. 24 (1999) 1434.
[13] H. Tsuchida, IEEE Photon Technol. Lett. 14 (2002) 513.
[14] R.P. Scott, C. Langrock, B.H. Kolner, IEEE J. Sel. Top. Quantum Electron. 7 (2001) 641.
[15] D. von der Linde, Appl. Phys. B 39 (1986) 201.
[16] D. Eliyahu, R.A. Salvatore, A. Yariv, J. Opt. Soc. Am. B 13 (1996) 1619.
[17] D.J. Derickson, A. Mar, J.E. Bowers, Electron. Lett. 26 (1990) 2026.
[18] H. Shi, I. Nitta, G. Alphonse, J. Connolly, P.J. Delfyett, Electron. Lett. 34 (1998) 2250.
[19] T. Yilmaz, C.M. DePriest, P.J. Delfyett Jr., Electron. Lett. 37 (2001) 1338.
[20] L.A. Jiang, M.E. Grein, E.P. Ippen, C. McNeilage, J. Searls, H. Yokohama, Opt. Lett. 27 (2002) 49.
[21] C.M. DePriest, T. Yilmaz, P.J. Delfyett Jr., S. Etemad, A. Braun, J. Abeles, Opt. Lett. 27 (2002) 719.
[22] T. Yilmaz, C.M. DePriest, P.J. Delfyett Jr., A. Braun, J. Abeles, Opt. Lett. 27 (2002) 872.
[23] M.E. Grein, L.A. Jiang, H.A. Haus, E.P. Ippen, C. McNeilage, J.H. Searls, R.S. Windeler, Opt. Lett. 27 (2002) 957.
[24] E. Yoshida, M. Nakazawa, IEEE Photon. Technol. Lett. 11 (1999) 548.
[25] W. Ng, R. Stephens, D. Persechini, K.V. Reddy, Electron. Lett. 37 (2001) 113.
[26] T. Yilmaz, C.M. DePriest, P.J. Delfyett Jr., J.H. Abeles, A. Braun, Proc. IEEE/LEOS Annu. Meet. 2 (2001) 906.
[27] H. Tsuchida, Opt. Lett. 23 (1998) 286.
[28] H. Tsuchida, Opt. Lett. 23 (1998) 1686.
[29] J.S. Wey, J. Goldhar, G.L. Burdge, J. Lightwave Technol. 15 (1997) 1171.
[30] O. Pottiez, P. Mégret, M. Blondel, IEEE Photon. Technol. Lett., submitted.
[31] T.F. Carruthers, I.N. Duling III, Opt. Lett. 21 (1996) 1927.
[32] R. Kiyan, O. Deparis, O. Pottiez, P. Mégret, M. Blondel, Electron. Lett. 34 (1998) 2410.
[33] R. Kiyan, O. Deparis, O. Pottiez, P. Mégret, M. Blondel, Opt. Lett. 24 (1999) 1029.